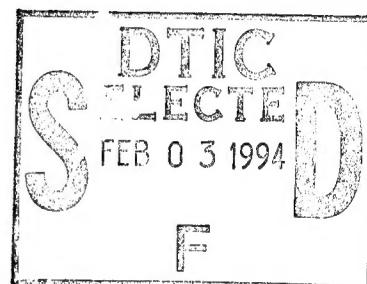# PROGRESS REPORT

(Year 1)

TO
OFFICE OF NAVAL RESEARCH

Design of a Fast-Tool Servo System using Magnetic Servo Levitation

by

Paul I. Ro, Associate Professor

Precision Engineering Center
North Carolina State University
Box 7918
Raleigh, NC 27695-7918
Tel: (919) 515-3096
Fax: (919) 515-3964
Internet: paul_ro@ncsu.edu

January 15, 1995

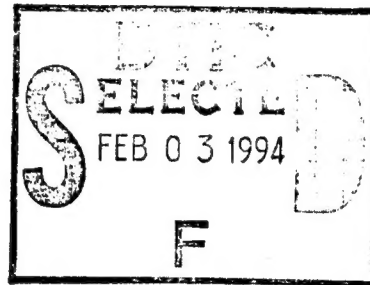# 19950130 111

1

PROGRESS REPORT

(Year 1)

TO

OFFICE OF NAVAL RESEARCH

Design of a Fast-Tool Servo System using Magnetic Servo Levitation

SELECTED
FEB 0 3 1994

F

North Carolina State University

Precision Engineering Laboratory

DESIGN OF A FAST TOOL SERVO SYSTEM USING MAGNETIC SERVO LEVITATION

Brent A. Stancil
Graduate Student
Hector Gutierrez
Graduate Student
Paul I. Ro
Associate Professor
Department of Mechanical and Aerospace Engineering
G. McDonald Moorefield, II
Research Associate

Magnetic Servo Levitation is proposed as a method to drive a Fast Tool Servo System, in order to compensate for errors resulting from mechanical misalignment, slide vibration, tool wear, and cutting dynamics on a Diamond Turning Machine. Theoretical magnetic equations have provided a basis for electromagnet design. Further analyses have used finite element models to find trends in magnetic properties, as well as assisting in structural design. A T-shaped, state-of-the-art composite structure has been proposed to transfer the electromagnet armature motion to the cutting tool. Flexural bearings are used to guide the T-structure as well as assist motion with their restoring force. Design of these are critical for the success of the servo. A static test fixture has been designed to investigate static forces as a function of coil current and separation gap of the electromagnet and armature. Results show very good correlation with theoretical values. A dynamic test fixture has been designed as well to determine limits in bandwidth, range, and positioning accuracy. Dynamics of the proposed system is discussed, along with simulation issues. Preliminary experimental data from the dynamic fixture is also presented.

INTRODUCTION

Magnetic Servo Levitation (MSL) [1] has been proposed as an alternative to piezoelectric actuators for the construction of a Fast Tool Servo System (FTS). The design objectives are (a) a range of 0.6 millimeters, (b) resolution on the order of nanometers, and (c) a 300 Hz bandwidth. MSL is free of friction and backlash problems accompanied by conventional mechanical actuators. Thus, the control scheme can be described mathematically and its behavior predicted quite accurately. Another desirable feature of MSL is the longer range of motion that can be obtained. Piezoelectric material is restricted in the sense that only a millistrain of elongation can occur through the whole crystal, so that a one meter long crystal is needed to produce one millimeter of travel. MSL uses the attractive force of electromagnets, and their limiting factor is that the force decreases at a rate of the separation gap squared as the electromagnet moves farther from the target. However, if designed properly, the actuation can easily obtain this travel.

The use of MSL for high precision positioning on the nanometer range is a promising but very challenging alternative to compensate for errors that can not be adequately handled by the cutting tool positioning control system. In most cases, the cutting tool positioning system tracks the position of the slide, and therefore cannot compensate for effects such as tool wear, spindle runout, slide vibration and the cutting dynamics. Fast-tool servo systems (FTS) are aimed to control such effects. In diamond turning, the motion range and bandwidth requirements makes conventional FTS systems unsuitable for this application.

While MSL should be able to provide an adequate bandwidth within a motion range twenty times larger than a piezo electric-based FTS, there is a number of fundamental issues that make difficult its implementation. An MSL based system is inherently unstable and highly non-linear. Controller design for an MSL system therefore requires a thorough understanding of the system's dynamics.

PART I: ACTUATOR DESIGN

I.1   ELECTROMAGNET DESIGN

I.1.1   Design Concept

The electromagnet will be constructed by using laminations of "E's" and "I's" (Figure 1) to produce a magnet-keeper system. Flexural bearings will be used to provide guidance of the armature and to provide a restoring force to return the armature to the center position. Issues to be addressed are magnet parameters, weight of moving mass, counterbalancing of the moving mass, flexure design, system modeling and amplifier selection.
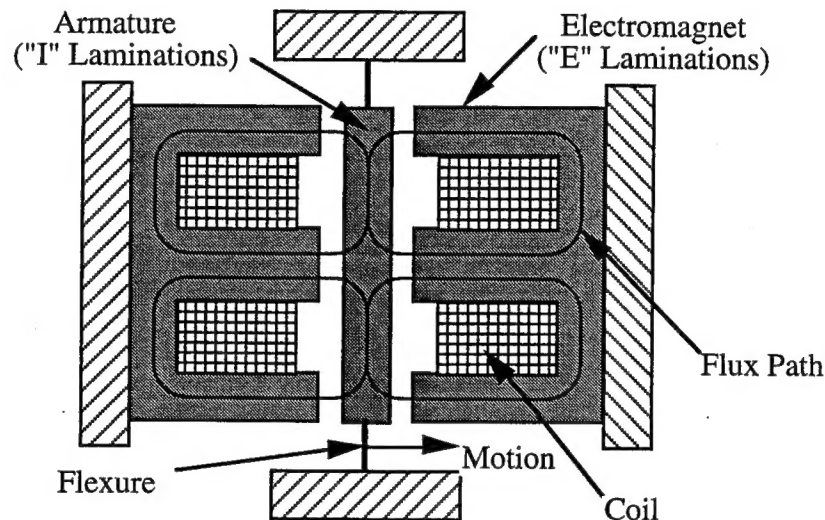

Figure 1: Electromagnet Concept

To obtain a starting point on the design of the electromagnetic system, theoretical electromagnetic expressions were used to determine the relationship between the resultant force and the electromagnet parameters. The starting point was to determine the reluctance, R, of the magnetic path.

$$R = \frac{l}{\mu_r \mu_o A} \tag{1}$$

where l is the length of the flux path, μ_r is the relative permeability of the core material, μ_o is the permeability of free space, and A is the cross-sectional area. Reluctance is analogous to resistance in an electric circuit, and is the resistance to the travel of the magnetic flux, Φ,

$$\Phi = \frac{Ni}{\Sigma R} = \frac{Ni}{\frac{1}{\mu_r \mu_o A} + \frac{2g}{\mu_o A}} \tag{2}$$

where N is the number of turns of wire on the coil, i is the current through the coil, and g is the gap between the "E" and "I" laminations. Once the magnetic flux has been determined, the inductance, L, of the coil can be obtained by

$$L = N \frac{\partial \Phi}{\partial i} = \frac{N^2 \mu_r \mu_o A}{1 + 2g\mu_r} \tag{3}$$

The energy, U, stored by the inductor is

$$U = \frac{1}{2} L i^2 = \frac{1}{2} \frac{N^2 i^2 \mu_r \mu_o A}{1 + 2g\mu_r} \tag{4}$$

and can be differentiated with respect to the air gap, g, to calculate F, the force produced by the single loop of flux.

$$F = -\frac{\partial U}{\partial g} = \left(\frac{N i \mu_r}{1 + 2g\mu_r}\right)^2 \mu_o A \tag{5}$$

Another consideration was that of magnetic saturation. The material chosen for the laminations, Orthosil M6, an iron-silicon alloy, has a saturation limit of 2 Tesla. Saturation places a plateau on the amount of force generated, by limiting the amount of flux generated, at the smaller gaps. The effect of saturation can be determined by

$$B = \frac{\Phi}{A} \tag{6}$$

where B is the flux density, which is the term containing the saturation value. However, saturation has a desirable effect as well. A smaller amount of current is needed to obtain saturation at the smaller gaps, therefore, the maximum current available from the amplifier is not needed to obtain the maximum force at these positions.

I.1.2 Electromagnet Parameters

A spreadsheet was developed to calculate the magnetic forces as a function of the dimensions and properties of the lamination material. Various gage wires were evaluated to determine the most suitable configuration. Force was not the final determining factor. Voltage, current, inductance, and the circuit's time constant played major roles as well in the final decisions. Allowable voltage

and current are limited by the amplifier used. Most commercially available amplifiers are restricted to outputs of approximately 50 volts and 15 amps. The time constant, τ, is defined by

$$\tau = \frac{L}{R} \qquad (7)$$

where R is defined as

$$R = \frac{\rho L}{A_w} \qquad (8)$$

and ρ is the resistivity of the wire, L is the length of the wire, and A_w is the cross-sectional area of the wire. The time constant is the time taken for the current to reach 63% of its projected value, and can be decreased by adding external resistance to the circuit. However, this may drive the voltage over the output limits of the amplifier. Smaller gage wire can produce larger forces due to the fact that more turns of wire can be placed on the same size bobbin. However, smaller wire has a higher resistance, resulting in higher required voltages, higher heat generation, and higher inductances. Force, being of the main concern, dominated this decision. The other side effects can be dealt with. The final design called for 400 turns of 26 gauge magnet wire, operating at less than two to three amps.

It was originally believed that the time constant of the magnetic circuit would increase if smaller wire was used and the number of turns increased. However, this was found not to be the case. All of the parameters needed to calculate the time constant all depend on the size of the bobbin used. Therefore, for a given bobbin that is totally filled with magnet wire, the time constant does not change with a change in wire diameter.

Because of hysteresis, stray magnetic field lines, etc., theoretical equations may not predict electromagnet performances accurately enough to totally rely on them for final design parameters. As a result, test fixtures have been built to study the static and dynamic characteristics of the electromagnets. The static test fixture compares the theoretical curves to the actual curves over a range of gaps and currents, similar to those generated by Poovey, Holmes, and Trumper [2]. The dynamic test fixture evaluates bandwidth, range of motion, and positioning accuracy by using a pair of electromagnets and an armature mounted on a single pair of flexures. These tests will prove if the goals can be achieved by the calculated parameters.

I.2   ANSYS MAGNETIC ANALYSIS

The finite element method was also used to evaluate the magnetic characteristics. ANSYS can be used to find the resultant magnetic forces, flux paths, and flux densities created by a specified magnetomotive force, N*i. The forces obtained from these analyses corresponded along those

values obtained from the theoretical calculations, and will not be repeated here. However, the analysis proved very useful in determining whether or not the direction of the flux paths in the magnet had any significant effect on the flux density. It was found that opposing flux paths "canceled" each other out, or their effects were not combined to cause a possible early saturation situation. However, if the flux paths ran in the same direction, their effect was additive, and created saturation at an early level. This is depicted below in figure 2.
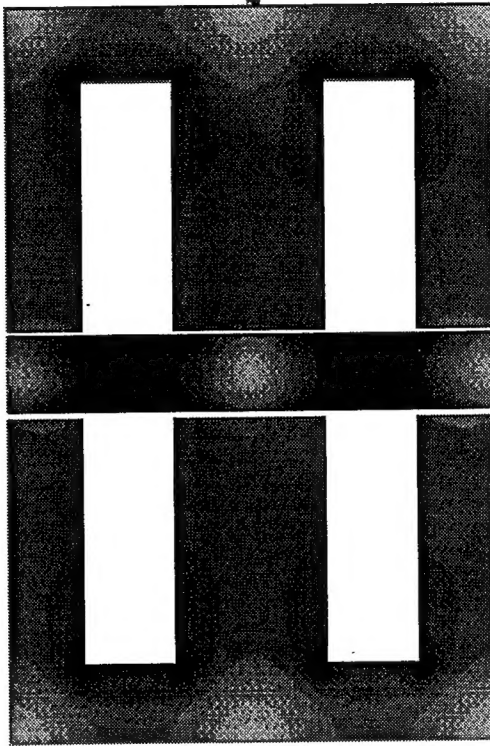

Figure 2: Sample ANSYS Figure Showing Flux Density

This analysis was for a current of 1.0 amps. This is about midrange of the current level that is being anticipated to be used. The darker areas show higher levels of flux density. As can be seen, even at the nominal gap and an average current, the flux density is very high for the case in which the flux paths run in the same direction. Analyses for which the flux paths oppose each other show that the B-field does not saturate as quickly, rather the paths act independently in creating flux.

I.3   EXPERIMENTAL RESULTS

I.3.1   Static Test Fixture

The static test fixture (figure 3) was designed so that the magnetic forces could be found accurately as a function of current and gap. Positioning of the electromagnet to the armature must be very accurate, therefore, mating surfaces and the electromagnet-armature interface were all ground. To keep flux losses to a minimum, the electromagnet and the armature were clamped into their casings by phenolic blocks pushed in by screws, and set by potting them with an electrical resin epoxy. To accurately measure the gap, a linear-variable differential transformer (LVDT) was used.
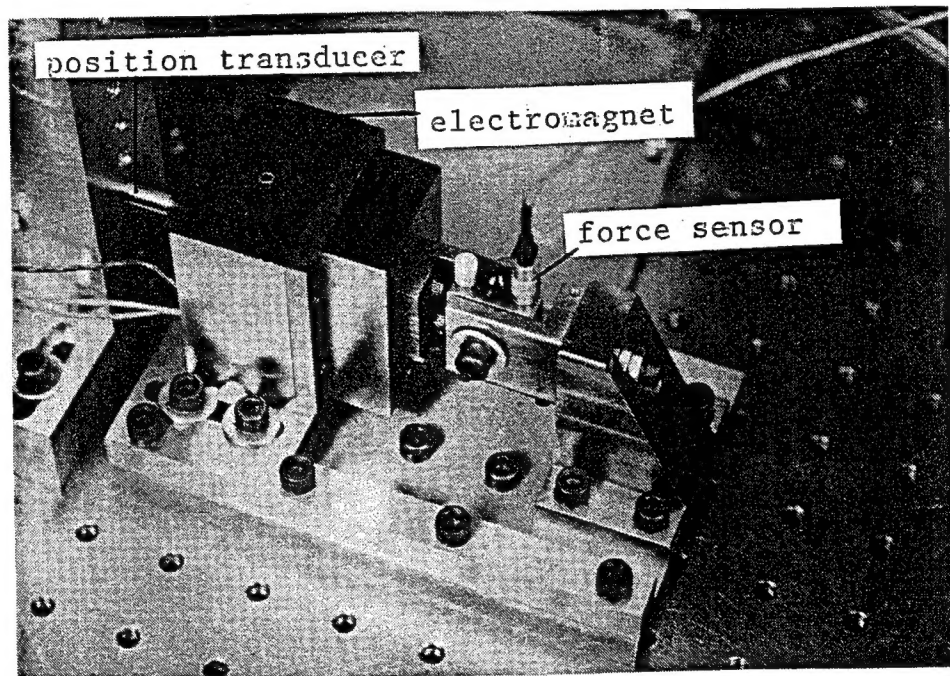

Figure 3: Static Testing Apparatus

Current was varied from zero to two amps, and the gap was incremented in 100 micron steps from 625 microns to 25 microns. However, in measuring the 425 micron gap a problem was encountered. As the electromagnet heats up, the epoxy appears to soften some. With the strength of the forces generated at larger current values, the electromagnet is pulled out of the epoxy slightly, but enough to not be able to reproduce previous results. It is not clear at this point whether this will be a problem later when the forces are pulsed on and off, rather than continuously on as they are in this test. Therefore, the results here will be for only the 625 and 525 micron gaps. Figures 4 and 5 compare the theoretical values calculated by Equation 5 and the experimental values.
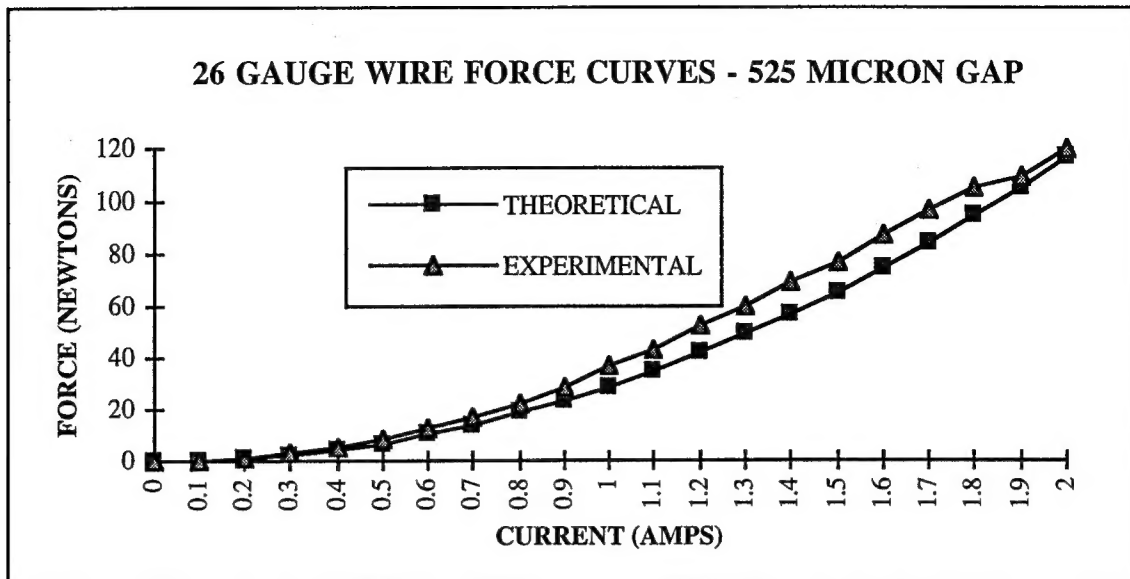
8

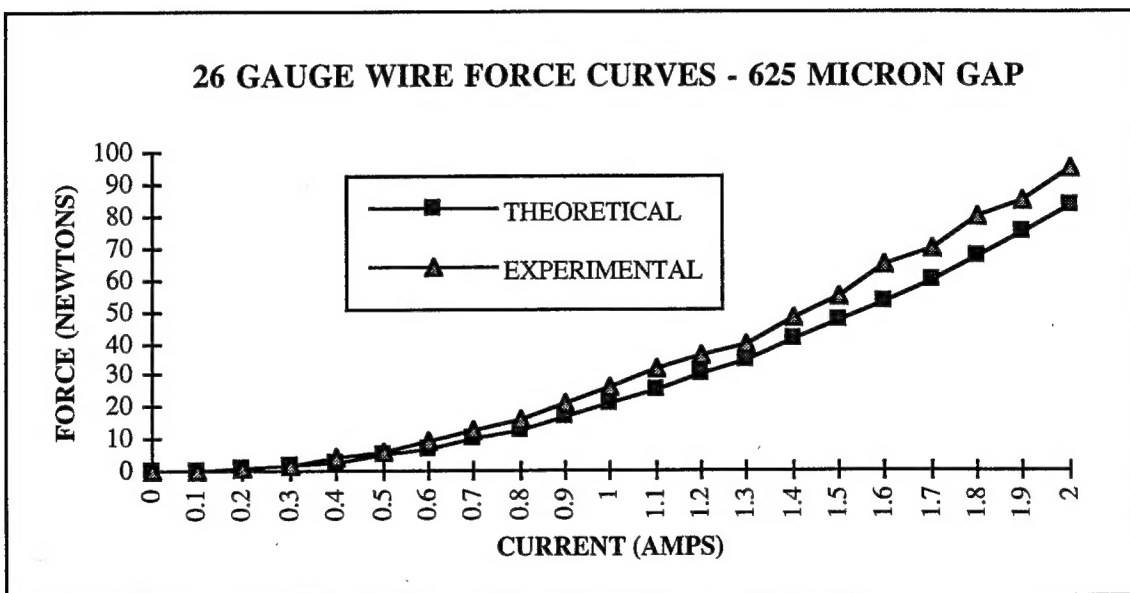**Figure 4:** Force Curves for 525 Micron Gap

Figure 5: Force Curves for 625 Micron Gap

These figures show an interesting trend. The experimental and theoretical values are very close to being the same. The experimental values are found by using an oscilloscope to measure the voltage output by a piezoelectric load cell. At the higher force readings, the scale on the oscilloscope is not as fine as that at the lower readings. Also, due to how accurate the magnet can be positioned, the actual gaps are usually slightly less than the value recorded for the experiment. The gaps are recorded as 625, 525, 425, etc. microns, rather than 612, 521, 415, etc. microns. These two observations may account for the variations found here. These results are very

encouraging, however, in the fact that the theoretical equations may can be used for modeling purposes. The remaining gaps will need to be evaluated to determine if this is possible.

I.3.2 Dynamic Test Fixture

The dynamic test apparatus (figure 6) was designed in the same fashion as the static apparatus. Two opposing electromagnets share an armature mounted on a pair of one-half inch long flexures. The natural frequency of the structure is about 123 Hz, and the stiffness is about 87.6 kN/m. The expected stiffness and frequency were higher than these numbers. This is because the supports were assumed to be perfect cantilevers. It has been noted that for cantilever supports, the effective length of the flexure should include half of the distance between the end of the support and the screws that clamp the two plates together. Using this effective length, the stiffness and natural frequency calculated by theoretical equations were very close to the actual values.
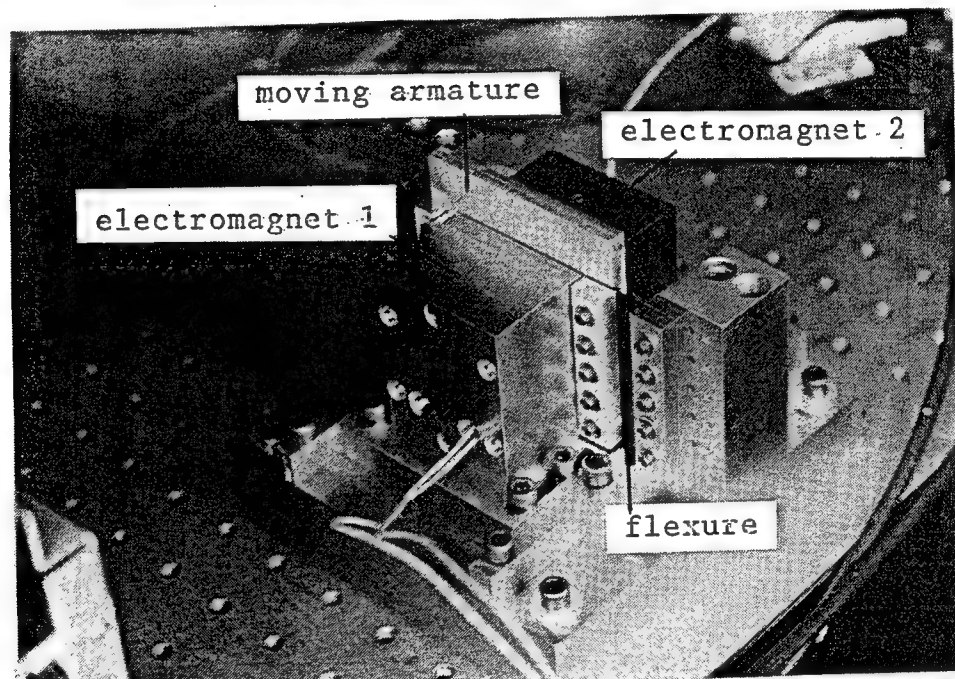

Figure 6: Dynamic Testing Apparatus

The goals of these experiments are to find a bandwidth, check positioning accuracy, help with modeling, and find a range of motion. These will be studied by first using an accelerometer mounted to the armature. The data is collected using LabVIEW, a data acquisition software package. A clipped sine-wave is input to both magnets, with alternating pulses going to each magnet. Then using MATLAB, the data can be analyzed to find the information needed. These tests are still being fine-tuned and have not delivered any acceptable data at this point.

I.4   STRUCTURAL DESIGN

Theoretical evaluations concluded that steel and aluminum structures would be too heavy given the desired bandwidth. Therefore, composite materials were investigated. The most appealing composite was carbon or graphite fiber reinforced plastics (CFRP and GFRP). It was found that several processes for obtaining these materials were being developed at North Carolina State University. The process that was chosen was a 3-D weave machine located at the College of Textiles. The product obtained has two-thirds the mass of aluminum, and has a specific modulus and specific strength more than twice that of steel and aluminum. The material is expensive to fabricate, but samples were obtained that can be used to produce an initial prototype. Most likely, steel will still need to be used to clamp the cutting tool on the structure, but it will not be a significant amount. The expected mass is about 0.227 kg.

The maximum inertia force needed to move the structure is about 250 N. This could lead to vibrations elsewhere on the DTM. Therefore, it is very possible that some sort of counterbalancing apparatus will be needed in the design.

The design of the flexures will prove crucial to the success of this project. The flexures provide guidance to the armature, as well as a restoring force to aid the electromagnets in pulling the armature back to the center position. The flexures must be designed so that they will provide sufficient restoring force, but not be so stiff that the electromagnets cannot overcome them. Also, the flexures must not compromise the system stiffness, since this will also affect the natural frequency of the system. If the actuator is to be operated with a 300 Hz bandwidth, the natural frequency of the system should be above 300 Hz.

The problem is then how the flexures should be sized. The actuator has been designed in a way so that it is stiff and lightweight (see Figure 7). Its structural dimensions are limited by its function, as well as mounting space, and cannot be varied. The material chosen is a stiff, lightweight graphite composite (modulus of elasticity of 70 GPa, and a density of 1525 kg/m^3). The flexures will not be excessively large, so spring steel can be used without worry of excess mass. A finite element model, using ANSYS, was developed to perform modal and static analyses of the proposed design.
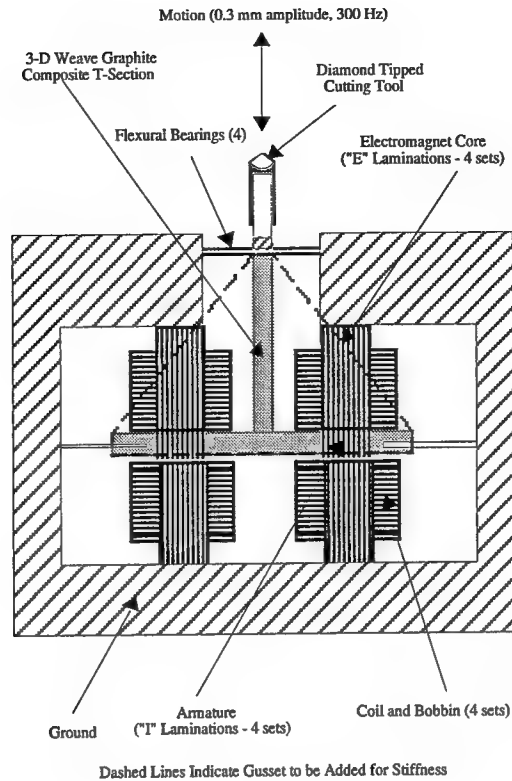
11

Motion (0.3 mm amplitude, 300 Hz)

3-D Weave Graphite
Composite T-Section

Diamond Tipped
Cutting Tool

Flexural Bearings (4)

Electromagnet Core
("E" Laminations - 4 sets)

Armature
("I" Laminations - 4 sets)

Coil and Bobbin (4 sets)

Ground

Dashed Lines Indicate Gusset to be Added for Stiffness

Figure 7: Actuator Design

The first step in the analysis was to develop a 2-D model of the system. This was done by using PLANE 42 plane stress elements, with thickness input. The dimensions were laid out by using variables for the various characteristic dimensions, so they could be changed with greater ease if needed later. The most important of these would be the flexure length and flexure width. The model was generated using keypoints and areas, after which the areas would be meshed. The areas were generated with ease of meshing in mind. This is why there is a thin strip of elements down the middle of the horizontal leg of the actuator (see Figure 8). This allows for easy transition between the two different materials. All nodes at the points where the flexures would be clamped in the ground were treated as cantilevered supports.
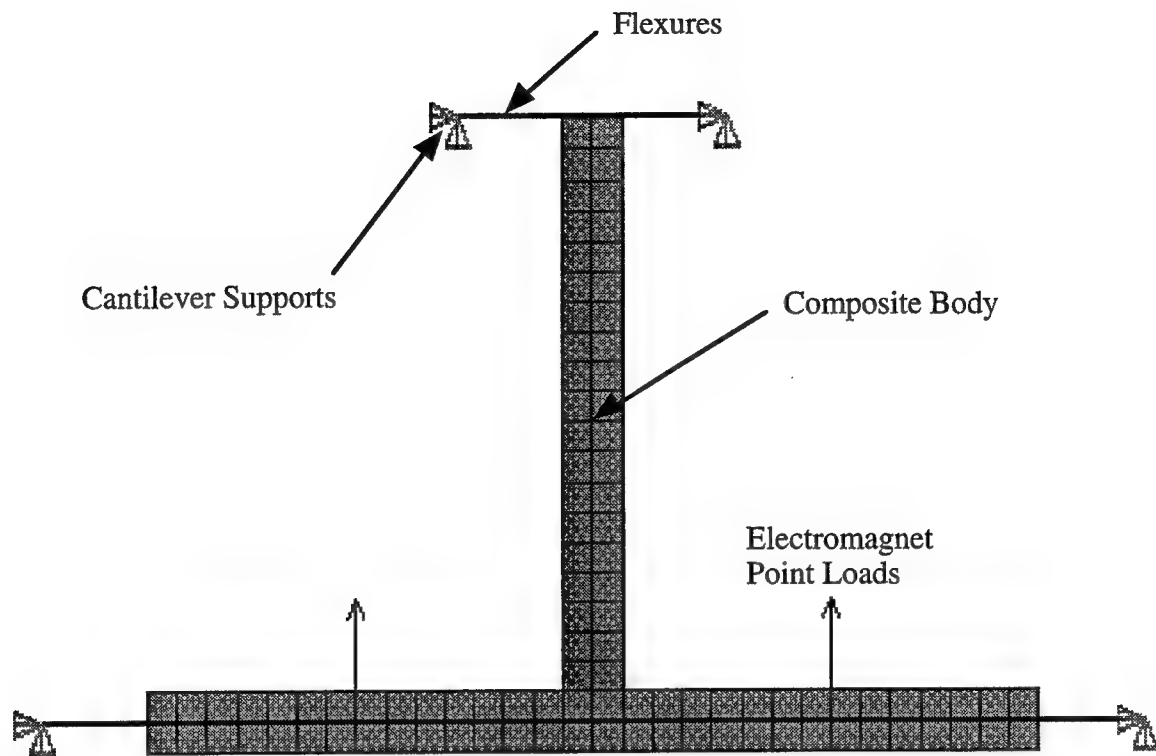
Figure 8: ANSYS Model

The modal analysis was solved using the Reduced (Householder) method. The amount of accuracy used in this method was sufficient enough, due to the other assumptions already taken in the model. Four modes were extracted to see where they occur and how the system will behave at the first four structural frequencies. A master degree of freedom was chosen at the middle of the structure, since this point should move in a straight line, and the program was allowed to choose 50 more. After this portion was solved, the solution procedure was run again to allow for the mode shapes to be printed.

A 3-D model was attempted to see how the gusset added to the top of the tee would effect the system. However, the model became too large for the computer resources available. It appears that educational versions of ANSYS have a maximum wavefront of 500 available. This model had a much larger wavefront. With further investigation of meshing techniques, this problem may be solved. The problem with the mesh seemed to have arisen due to the triangular nature of the gusset. Even though an element size of 2.8 mm (7/64 in) was selected, much smaller elements were created, as well as poorly shaped elements, in order to get the triangle meshed.

A static analysis was then performed on the modal analysis model. Point loads were applied where the magnets would pull on the actuator. These loads were varied until the structure was displaced 300 microns. Also, the stresses were evaluated in the flexures and tee.

The original mesh of element sizes of 2.8 mm (7/64 in) proved adequate in the analysis. A very small change was noticed in any further refinements, therefore, the larger mesh was retained. Increasing the thickness of the flexures to more than 0.25 mm (0.010 in) made them too stiff for the electromagnets to overcome. Therefore, the only variable remaining in the analysis was the length of the flexures. These results are seen in Table 1.

Flexure Length	Force Req'd to Move 300 microns	First Mode	Second Mode	Third Mode	Fourth Mode
9.5 mm (0.375 in)	142 N/magnet (32 lbf)	595 Hz	1994 Hz	4762 Hz	8016 Hz
11.1 mm (0.4375 in)	93 N/magnet (21 lbf)	473 Hz	1888 Hz	4661 Hz	7944 Hz
12.7 mm (0.500 in)	62 N/magnet (14 lbf)	383 Hz	1816 Hz	4563 Hz	7806 Hz

Table 1: ANSYS Results

The maximum force put out by the electromagnets is about 200 N. This eliminates the 9.5 mm (0.375 in) flexures, because there will be little force left to accommodate the inertial forces required for the system. The first mode of the 12.7 mm (0.500 in) flexures is too close to 300 Hz to feel comfortable with, therefore, the 11.1 mm (0.4375 in) flexures were chosen to be the design choice.

These results need to be compared to some sort of theoretical model to justify the analysis. The best way to model the flexures are as cantilevered beams with guided ends. Since all the flexures see the same deflection, they are all in parallel, and the equivalent stiffness is four times that of one flexure. Finally, the tee was assumed to be infinitely stiff as compared to the flexures. The following equation was used to calculate the stiffness of the system:

$$k_{eq} = 4 * \frac{12\,E\,I}{l^3} \tag{9}$$

This result from ANSYS was 623 N/mm, and the result from equation (9) was 596 N/mm. Therefore, the analysis was justified.

The plots of the mode shapes may justify not needing a gusset on top of the tee. The first mode results in simple 1-D motion. Only in the higher mode shapes do 2-D deflections show up. Since the system is not expected to be operated where these mode shapes occur, the tee should be fine the way it is. Having the flexures at the end at which the tool is attached assists in keeping the structure from deflecting side to side.

Finally, the stresses in the flexures may be of some concern. Spring steel has a yield strength of 400 to 1650 MPa. Principle stresses at the edges of the flexures were 345 to 400 MPa. If the spring steel used is of at least the middle range strength, the design should be fine. However, fatigue loading should also be considered. The stresses observed in the composite material was negligible.

I.5   SYSTEM SIMULATION

Another approach to the system design is to model the structure on MATLAB. The system without the electromagnets can be modeled as a single degree of freedom, spring-mass system

$$M\ddot{x} + B\dot{x} + Kx = F(x) \tag{10}$$

where M is the mass of the system, B is the damping in the system, K is the system stiffness, and F(x) is the external forcing function.

The major issue to be addressed here is how the effect of the resonant peak on the system response can be minimized. It appears that the peak will be very close to, if not within the bandwidth of the system. Therefore, some way must be found to handle this. One possible way is through proportional-derivative (PD) control. Once this entry level model has been perfected, the electromagnets can then be brought into the system equation and be tested.

PART II: DYNAMICS OF A MAGNETIC SERVO-LEVITATED FAST-TOOL SERVO SYSTEM

II.1 MATHEMATICAL MODELING AND SIMULATION

II.1.1 Mathematical model

The system under consideration consists of two electromagnets driving a moving element supported by elastic flexures, as depicted on figure 9.
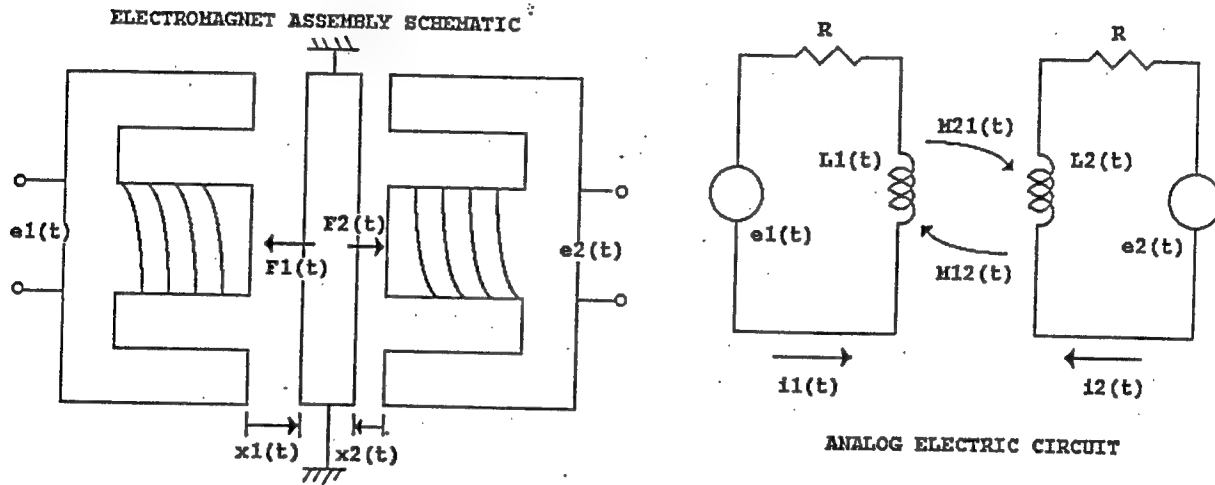

Figure 9: Schematic of the MSL system and corresponding analog electric circuit

$L_1(t)$, $L_2(t)$ represent the inductance of each coil, $M_{12}(t)$, $M_{21}(t)$ are the corresponding mutual inductances; $e_1(t)$, $e_2(t)$ are the input voltages; and $x_1(t)$, $x_2(t)$ define the position of the moving element. Notice that in this case $x_1(t)+x_2(t) = 0.00105$ m. Assuming that the input to the electromagnets are ideal voltage sources, the circuit equations are given by:

$$-L_1 \frac{di_1}{dt} - M_{12} \frac{di_2}{dt} - Ri_1 + e_1 - i_1 \frac{dL_1}{dt} - i_2 \frac{dM_{12}}{dt} = 0 \tag{11}$$

$$-L_2 \frac{di_2}{dt} - M_{21} \frac{di_1}{dt} - Ri_2 + e_2 - i_2 \frac{dL_2}{dt} - i_1 \frac{dM_{21}}{dt} = 0 \tag{12}$$

On the other hand, the magnetic forces are given by the partial derivative of the total magnetic energy stored in the system with respect to the displacement, i.e.:

$$F_1 = -\frac{1}{2} i_1^2 \frac{\partial L_1}{\partial x_1} \quad ; \qquad F_2 = -\frac{1}{2} i_2^2 \frac{\partial L_2}{\partial x_2} \tag{13,14}$$

$$F_1 = -\frac{1}{2}i_1^2\frac{\partial L_1}{\partial x_1} \quad ; \quad F_2 = -\frac{1}{2}i_2^2\frac{\partial L_2}{\partial x_2} \tag{13,14}$$

Notice that L depends also on the current (in the more general case, when the magnetic core can be saturated), but the force is defined for a given value of i.

The state-space equations are thus defined as follows:

$$\frac{di_1}{dt} = f_1(i_1, i_2, x_1, \frac{dx_1}{dt}) \qquad \frac{di_2}{dt} = f_2(i_1, i_2, x_1, \frac{dx_1}{dt})$$

$$\frac{dx_1}{dt} = x_0 \qquad \frac{dx_0}{dt} = \frac{1}{m}[F_2 - F_1 - 2k(x_1 - 0.000525)] \tag{15}$$

where the first two equations are obtained by solving (11) and (12) for di_1/dt and di_2/dt, the fourth state (x_0) represents the speed of the moving element, and its derivative is given by the total force acting on it. The spring force is given by k (spring constant).
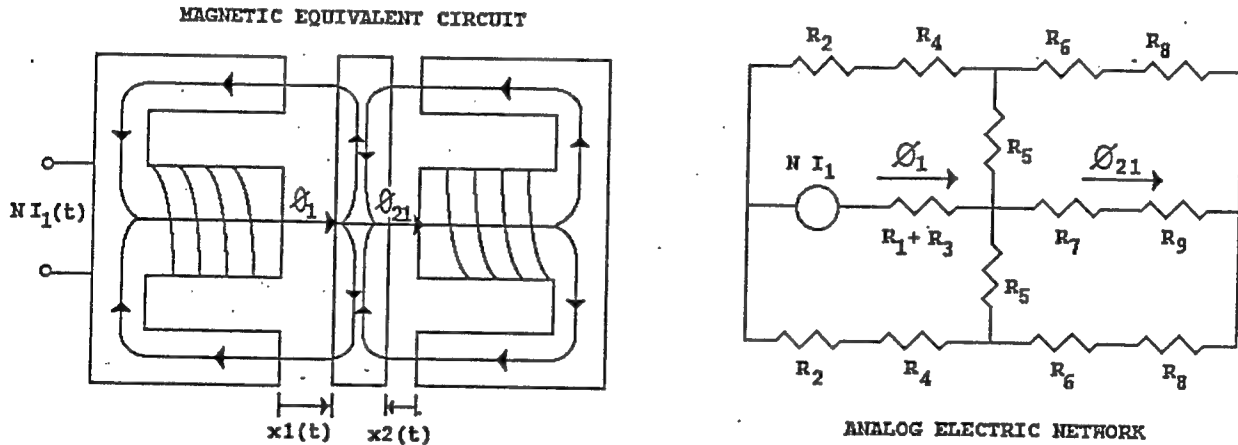

Figure 10: Magnetic equivalent circuit and analog electric network

The next step consisted on estimating the physical parameters involved in the aforementioned equations. To obtain dependable expressions for the inductances and mutual inductances is no trivial task. Strictly speaking, autoinductance is defined as two times the derivative of the total magnetic energy with respect to i^2. Assuming that there is no magnetic flux loss (i.e., assuming that all the magnetic energy is stored both on the gap and the core), we can say:

$$L_i = N\frac{\partial \phi_i}{\partial i_i} \qquad M_{ji} = N\frac{\partial \phi_{ji}}{\partial i_i} \tag{16}$$

17

Here $\varnothing_i$ represents the magnetic flux originated on coil i that links coil i, and $\varnothing_{ji}$ represents the flux originated on coil i that goes through coil j, for i,j= 1,2. This simplified calculation requires to compute the magnetic flux on each magnet and that requires further assumptions.

In order to estimate L and M, an approximated calculation based on the corresponding magnetic circuit was carried out. The magnetic equivalent circuit is depicted on figure 10. Assuming that the field density (B) is uniform over any given section of the magnetic core, and that the magnetic intensity (H) is constant over any given segment of the same material along the mean magnetic path, the reluctance of the ith segment of the magnetic circuit is given by:

$$\Re_i = \frac{l_i}{\mu_i A_i} \quad ; \quad where \quad \mu_i = \frac{B_i}{H_i} \quad , \quad B_i = \frac{\phi_i}{A_i} \quad\quad\quad (17)$$

The parameter estimation is performed by a computer program for a given set of values of x_1, x_2, i_1, i_2. First, a small value of B is assumed. Then, the permeability (μ) is interpolated from a look-up table of points taken from the actual B-H curve of the material under consideration. Then, the total reluctance is obtained (from the analog electric network, figure 10), and, for the given magneto-motive forces (Ni_1, Ni_2), the flux can be obtained and therefore B (according to (17)). The final B is compared to the initial guess, and if the difference is greater than some threshold value, the guess will be increased on a small amount and the computation is repeated. This algorithm is fairly slow if a reasonable accuracy is expected.

The source of non-linear behavior and parameter uncertainty on a MSL system is given by the relationship between voltage applied to coils 1 and 2 and the force exerted upon the moving element.

II.1.2 Parameter estimation verification

The computation described above requires a number of simplifications. In order to obtain a better estimate of the electrical parameters, a finite-element based calculation was performed. This takes into account both magnetic flux losses and the non-uniform nature of the distribution of B and H within the magnetic core. The limitation is given also by a major assumption: the software used (Maxwell-Ansoft) solves the problem on a cross section, assuming the actual system is extended infinitely in the direction perpendicular to the paper. In spite of this, its results should be significantly more accurate than the calculation described above. Another main limitation on the use of finite-element methods is computation effort: for a single set of currents and positions, the program may take several hours to converge. An example run of this computation is shown in figure 11. Notice that there is a significant flux fringing between the two inmost flux lines on each coil. This shows that a significant amount of energy is stored outside the gap and therefore the actual inductance must be greater than the value obtained from the calculation described before. For

18

the set of conditions on figure 11, the simplified calculation predicts L_1= 30.8 mH; a finite-element based calculation yields L_1= 53.8 mH. Notice that the actual inductance is even larger than this, since there is fringing on the third dimension that the finite-element software do not take into account.
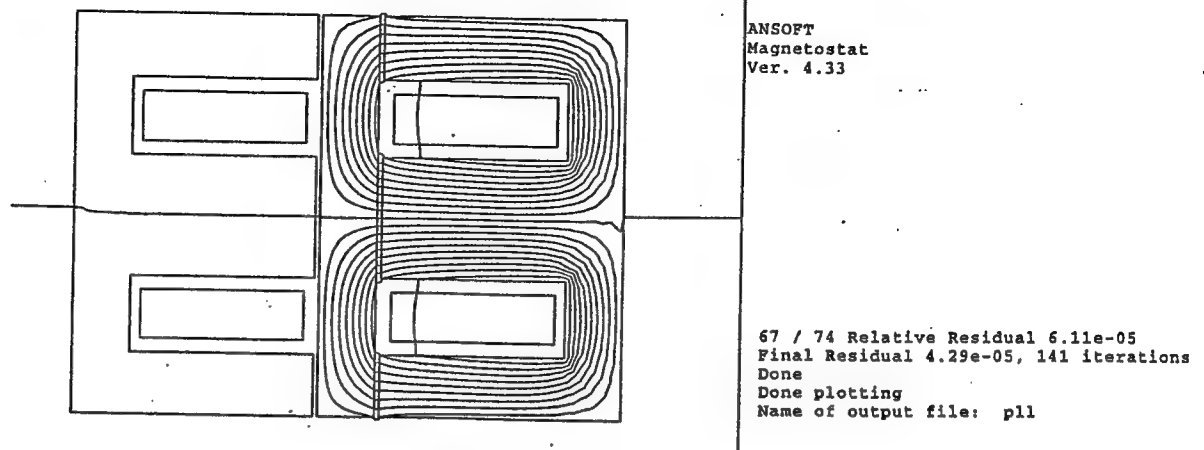


```
ANSOFT
Magnetostat
Ver. 4.33


67 / 74 Relative Residual 6.11e-05
Final Residual 4.29e-05, 141 iterations
Done
Done plotting
Name of output file:  pll
```

Figure 11: Finite-element estimation of the inductance. The lines show the magnetic flux lines under the following conditions: x_1= x_2= 0.000525 m., i_1= 0 A, i_2= 0.9 A. The inductance is obtained from the total magnetic energy stored in the system

II.1.3 Computer Simulation

A computer simulation was implemented based on the system's equations described on section II.1.1. A schematic of this implementation is shown in figure 12. The inputs are voltages e_1, e_2; the state equations (15) are implemented in the block labeled plant3.
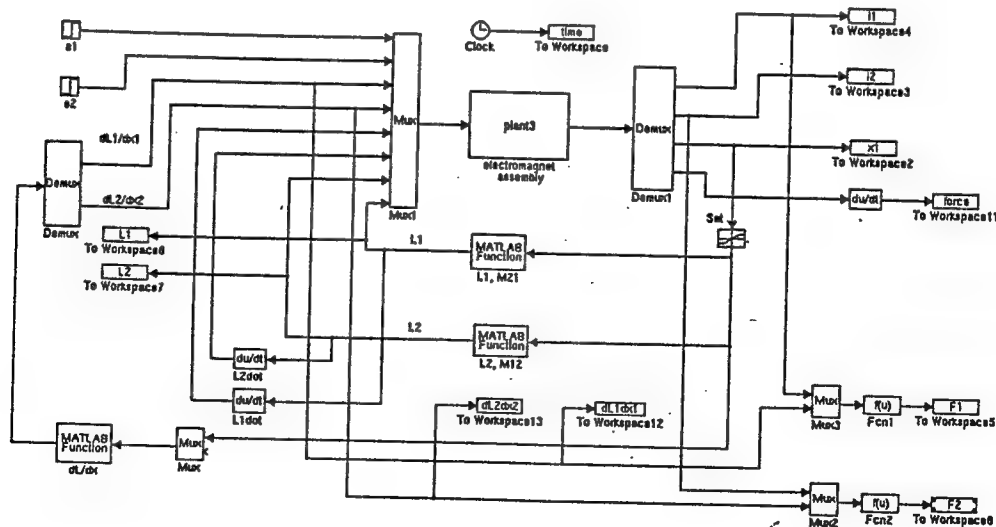

Figure 12: Computer simulation network

19

The computationally intensive part of each iteration is the parameter estimation. For each value of the state vector [i_1, i_2, x_1, dx_1/dt], the autoinductances and mutual inductances are estimated as described before. It was determined (both from the iterative computation and using finite-element methods) that the mutual inductances are approximately three orders of magnitude smaller than the auto inductances; the corresponding terms on equations (11), (12) were thus neglected.

A simulation run gives an interesting insight about the dynamics of this system. Simulated results are shown in figure 13 for the following set of conditions: at t=0, the current i_1 is zero and i_2= 1.8 A. The moving element is hold still at x_1= 0.001 m. Then the voltage in coil 2 is dropped to zero and an step voltage is applied to the first coil in order to reach an steady-state current equal to 12 A.
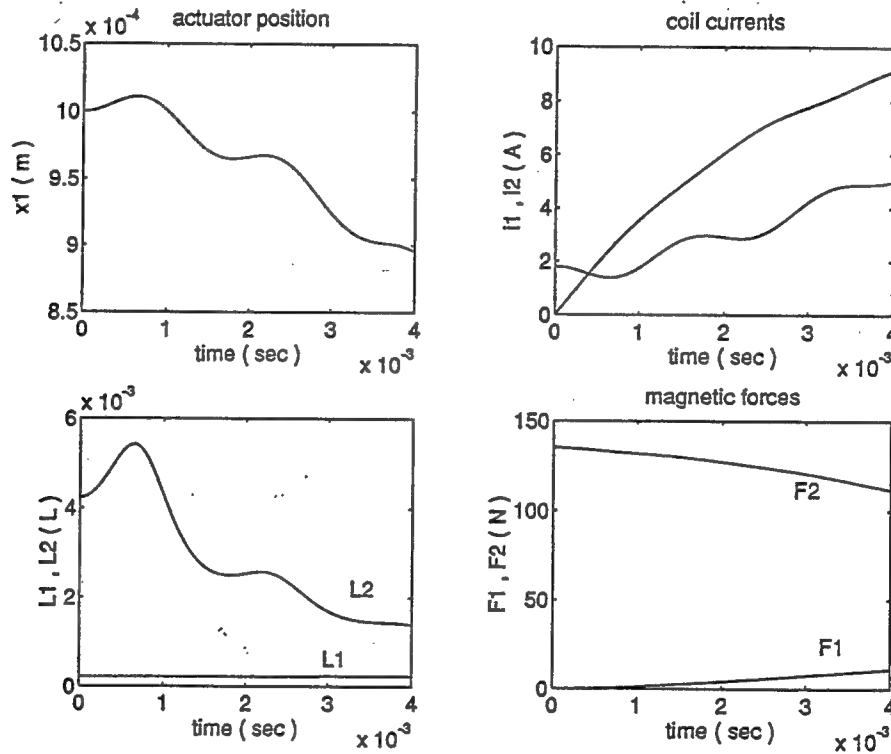

Figure 13: Computer simulation results

The moving element starts moving towards magnet 1, oscillating with a frequency given by the square root of k/m. Notice that the magnetic forces change slowly when the moving element is close to one of the magnets. This is because this force is proportional to dL/dx, and this derivative is close to zero when the element is far from the corresponding magnet (see L_1). Therefore, in the extreme positions, the spring plays a critical role in determining the motion.

To understand the behavior of the coil currents, we need to consider the dynamics of the electric circuit. Consider for example (11). Neglecting the mutual inductances, we get:

$$-L_1 \frac{di_1}{dt} - Ri_1 + e_1 - i_1 \frac{dL_1}{dt} = 0 \tag{18}$$

This can be solved to yield an analytic solution for i_1. This is (for each coil):

$$i(t) = \frac{i_0 L_0}{L(t)} e^{-\frac{R}{L}t} + \frac{e^{-\frac{R}{L}t}}{L(t)} \int_o^t e(t') \exp(\frac{R}{L}t') dt' \tag{19}$$

where $e(t)$ is the corresponding input voltage to the coil, and i_0, L_0 are initial conditions. For $e(t)=$ 0 for $t > 0$, the second term disappears. This explains how even after disconnecting the voltage on coil 2, the current i_2 can still go up: since L_2 is dropping (with respect to L_0), there is a factor greater than 1 multiplying the exponential term, which tends to 1 for small values of t.

It is also important to notice that the time constant of the system is very large due to the inductances: for the given initial conditions, the time constant of circuit 1 is estimated as 3.6 msec; for circuit 2 (the one being disconnected) the time constant is 144.2 msec, and therefore it can take as much as 1.44 sec to reach steady state current. A high time constant represents an important physical restriction to control this type of system: any desired output will have a considerable delay before reaching steady state. Moreover, this delay will be different on both circuits and is also dependant both on the current position of the moving element and the present currents on both circuits.

II.2 CONTROLLER DESIGN: DYNAMIC LINEARIZATION

II.2.1 Full-state feedback approach based on dynamic linearization

The more straightforward approach to controller design for MSL is to develop a linearized version of the system's equations in order to use linear controller design techniques. The first attempt to linearize the system was done based on the fact that there is a known trajectory around the equilibrium position (x_1=0.000525 m), and that is $x_1(t) = x_2(t) = 0.000525$, for the input vector $[e_1(t)\ e_2(t)] = [0\ 0]$. Assuming that the system's range of motion can be covered according to trajectories generated by small perturbations on these initial conditions, the system's dynamics around the equilibrium trajectory can be described by the dynamics of such perturbations, i.e.:

$$\frac{d}{dt}\begin{bmatrix} z_1 \\ z_2 \\ z_3 \\ z_4 \end{bmatrix} = \begin{bmatrix} \dfrac{\partial f_1}{\partial i_1} & \dfrac{\partial f_1}{\partial i_2} & \dfrac{\partial f_1}{\partial x_1} & \dfrac{\partial f_1}{\partial x_0} \\ \dfrac{\partial f_2}{\partial i_1} & \dfrac{\partial f_2}{\partial i_2} & \dfrac{\partial f_2}{\partial x_1} & \dfrac{\partial f_2}{\partial x_0} \\ \dfrac{\partial f_3}{\partial i_1} & \cdots & \cdots & \cdots \\ \cdots & \cdots & \cdots & \dfrac{\partial f_4}{\partial x_0} \end{bmatrix} \begin{bmatrix} z_1 \\ z_2 \\ z_3 \\ z_4 \end{bmatrix} + \begin{bmatrix} \dfrac{\partial f_1}{\partial u} \\ \dfrac{\partial f_2}{\partial u} \\ \dfrac{\partial f_3}{\partial u} \\ \dfrac{\partial f_4}{\partial u} \end{bmatrix} v \qquad (20)$$

where $[z_1\ z_2\ z_3\ z_4]$ is the vector of state perturbations, f_1, f_2 are defined as in (5), $f_3 = x_0(t)$ and $f_4 = dx_0/dt$ corresponds to the force equation in (15); $v(t)$ is an scalar input function. Notice that even though (from a modeling point of view) the system has two inputs, from a control perspective it can be considered only one, since achieving some desired trajectory requires the excitation to both coils be coordinated. For example $e_1(t) = u(t) + e_0$; $e_2(t) = u(t) - e_0$, for some e_0 constant.

Equation (20) thus determines a linear time-variant system: $dZ/dt = AZ + Bu$ around the aforementioned equilibrium trajectory. Assuming that (for small displacements) each new state can be considered a quasi-equilibrium point, the state matrix A can be updated so that the linearization can be extended to the whole operating range.

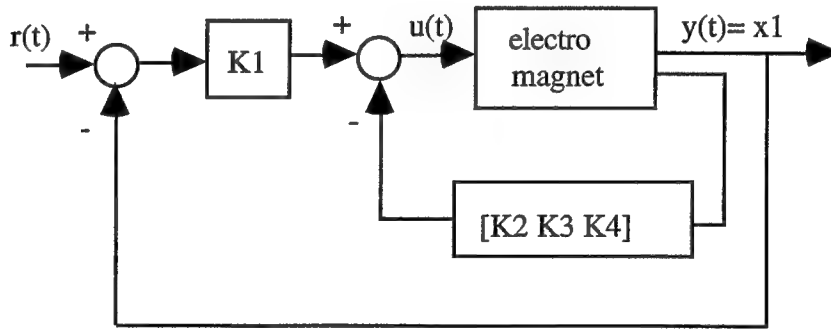With this in mind, a pole placement-based scheme can be implemented as in figure 14.

Figure 14: Full-state feedback control

where $[K_1\ K_2\ K_3\ K_4]$ is a gain vector obtained using pole-placement and the linearized model (20), which is updated at every iteration depending on the current values of the states; $r(t)$ is an arbitrary trajectory to be tracked.

The root locus of the linearized system, for the initial conditions described on the previous section, is shown on figure 15. There is a pole-zero cancellation on the negative real axis, and this makes the system unobservable under those conditions.
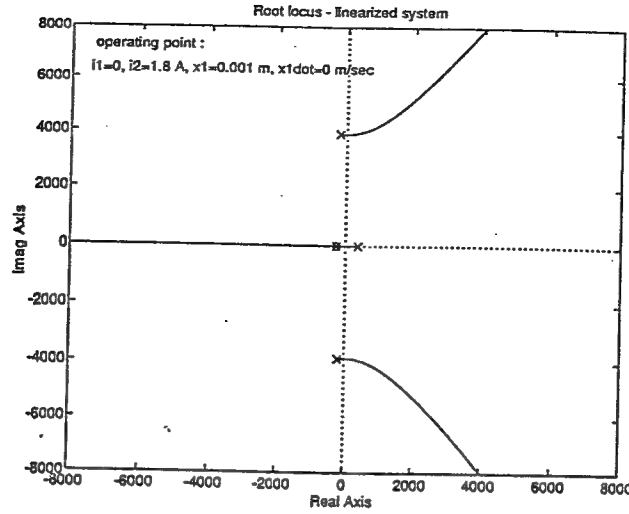
22

Figure 15: Root locus of the linearized system. The initial conditions are the same as in figure 13.

The main limitation on this approach resides on the assumptions of both small displacements and quasi-equilibrium. Besides, the control action u(t) should be small compared to the bias level e_0. The state matrix changes according to the current value of the states, and it has been observed that the system can loose either controllability or observability or both for a given set of state values. Thus pole placement would not be applicable, since it requires both observability and controlability along the range of motion.

II.2.2 Algebraic linearization

A second approach is based on finding the bias currents i_{1o}, i_{2o} that would make the system to follow linear dynamics. The control signal would then be computed according to linear controller design techniques and applied as a perturbation to the bias signal. For instance, we would like to express the magnetic forces as:

$$-F_1 = \frac{K_p i_1^2}{x_1^2} = B_1 \frac{dx_1}{dt} + K_1 x_1 \tag{21}$$

$$-F_2 = \frac{K_p i_2^2}{(1.05x10^{-3} - x_1)^2} = B_2 \frac{dx_1}{dt} + K_2 x_1 \tag{22}$$

where K_p is a physical constant of the system and B_1, B_2, K_1, K_2 are some unknown design parameters. For example, for a given desired natural frequency and damping ratio, we would have:

$$\omega_n = \sqrt{\frac{K_2 - K_1 + 2k_0}{m}} \quad ; \quad 2\xi\omega_n = \frac{B_2 - B_1}{m} \tag{23}$$

Assuming B_1, B_2, K_1, K_2 can be obtained, the linearizing bias currents would be:

23

$$i_{1_0} = \frac{x_1}{\sqrt{K_p}} \sqrt{B_1 \frac{dx_1}{dt} + K_1 x_1} \qquad\qquad (24)$$

$$i_{2_0} = \frac{(1.05x10^{-3} - x_1)}{\sqrt{K_p}} \sqrt{B_2 \frac{dx_1}{dt} + K_2 x_1} \qquad\qquad (25)$$

which would yield the following system's dynamics:

$$m\frac{d^2 x_1}{dt^2} + (B_2 - B_1)\frac{dx_1}{dt} + (K_2 - K_1 + 2k_0)x_1 = 2k_0 x_d = 1.05x10^{-3}k_0 \qquad\qquad (26)$$

where m is the mass of the moving element, k_0 the spring constant of the support flexures, and x_d defines the equilibrium position. This approach needs to be further investigated.

II.3 DYNAMIC TEST

II.3.1 Description of the test set-up

A dynamic test was carried out to gather data that could be used for model validation (through computer simulation), system identification and neural network training. The experiment was aimed to generate sinusoidal motion on the moving armature by applying sequences of half-wave rectified sine waves to the power amplifiers that drive the magnets.
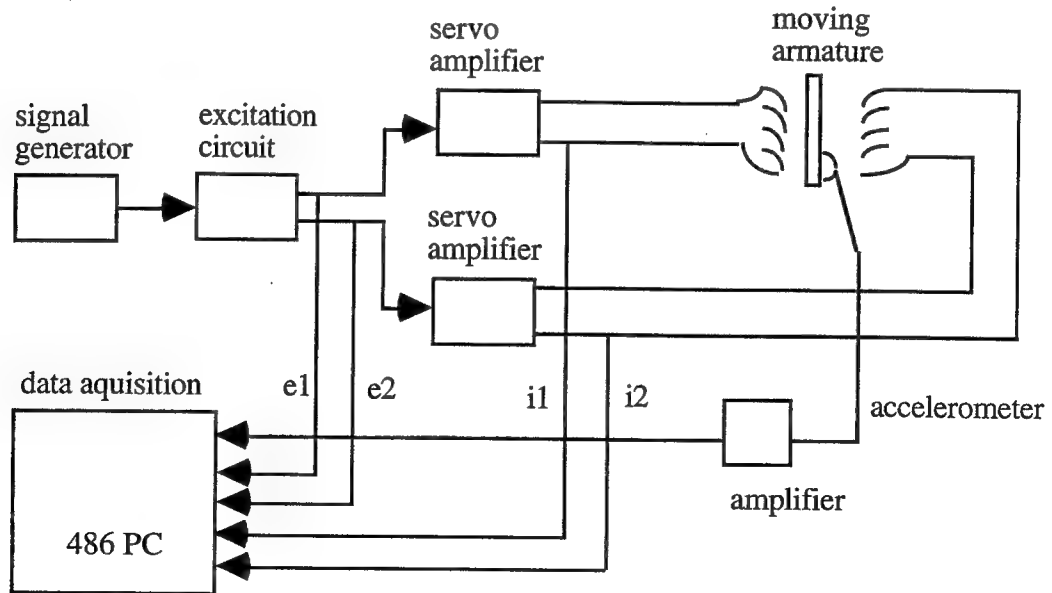

Figure 16: Dynamic test- Experimental set-up

24

The experimental set-up is shown on figure 16. The signal generator provides a sine wave of a given frequency. The excitation circuit alternates this signal such that one servo amplifier gets excitation signal while the other is off; this will be further explained in the following section. The input voltage to both servo amplifiers is recorded, along with the corresponding currents on the electromagnets and the acceleration on the moving armature.

II.3.2 Excitation circuit

The excitation circuit is depicted on figure 17. The need for this circuit comes from the fact that the excitation on both coils needs to be alternated in order to generate a desired motion. This will be more evident when examining the results, in the next section.
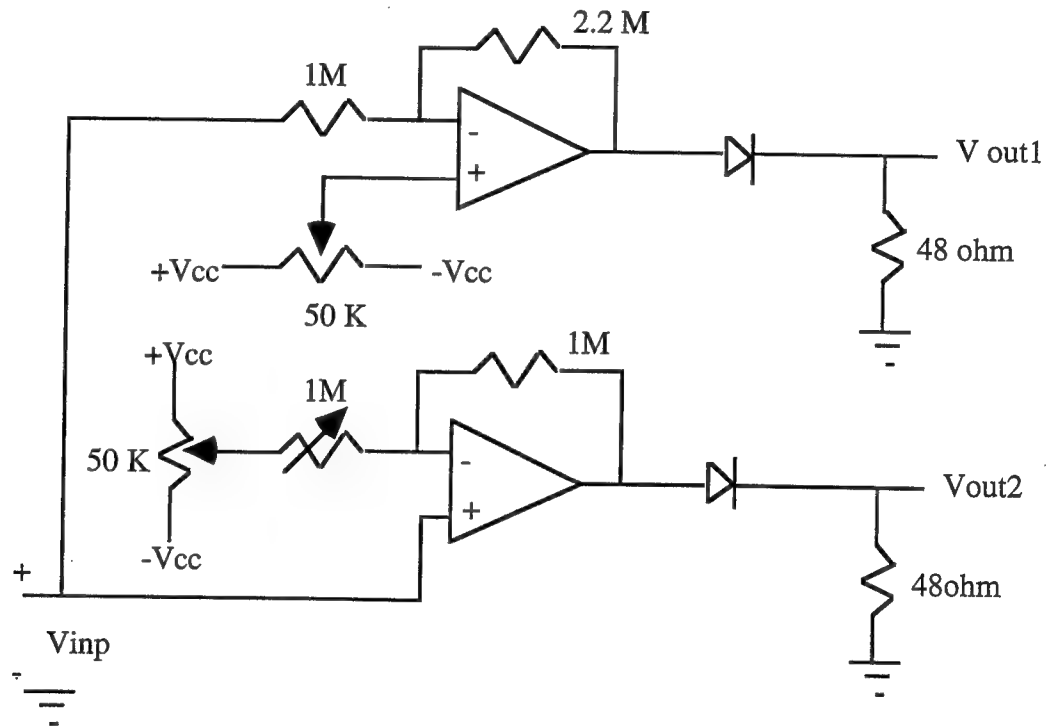
Figure 17: Excitation circuit

The input signal is sent through two operational amplifiers, one of them configured as an inverter amplifier in order to introduce a 180 degree phase between the corresponding outputs. There are two 50K potentiometers used to null the offset output voltage, and one 1M potentiometer used to calibrate both amplifiers to the same gain. The output resistor was chosen to match the input impedance of the servo amplifiers.

II.3.3 Results

The experiment was run at four different excitation frequencies: 3 Hz, 30 Hz, 300 Hz and 500 Hz. The corresponding sampling frequencies were 5 KHz, 20 KHz, 20 KHz and 20 KHz. Results are shown in figure 18. Consider for example the plot corresponding to 30 Hz. The alternating pulses corresponding to half of a sine wave correspond to the input voltages (e_1, e_2) generated by the excitation circuit. The currents on each magnet (i_1, i_2) can be easily matched with the corresponding excitation voltages since the current pulses are shifted and slightly distorted with respect to the original sine wave pulses. The fifth trace on each plot correspond to acceleration data. The same convention of line types applies to all four plots (see figure 18).

The oscillatory movement is clearly illustrated at 300 and 500 Hz. At 3 Hz, the acceleration data becomes out of range since the moving armature banged on the fixed frame at each oscillation.

The amplitude spectra of the data sets at 300 and 500 Hz are shown in figure 19. Both of them present distinctive peaks corresponding to the excitation frequency. In the plot corresponding to 500 Hz there are also other lobes that seem to correspond to the mechanical structure natural frequency and its harmonics. Close after 1000 Hz on this plot there is a resonant peak where both the harmonics of the excitation signal and the mechanical natural frequency seem to correspond.

II.4 MODEL EVALUATION

II.4.1 Modifications on the simulation network

Since we are primarily interested on studying the dynamics of the MSL system, a second simulation network was set in order to test the mathematical model described on a previous section by comparing it to the experimental results. The input to the model will be the measured current, and the corresponding output will be acceleration, in such a way that model-predicted acceleration can be directly compared to actual data. The modified network is illustrated on figure 20.

On this implementation, the non-linear plant has two states (position and velocity) and two inputs (currents). The input sequences are retrieved from the workspace and correspond to experimental data; the predicted acceleration is written to a workspace variable too. The non-linear nature of the core is considered on the block that computes the derivative dL/dx: this routine calls the iterative functions that predict inductances (as described on a previous section) as a function of both the position and the coil currents. The non-linearity given by the magnetic force is included on the state equations (plant block) as in the previously described network.
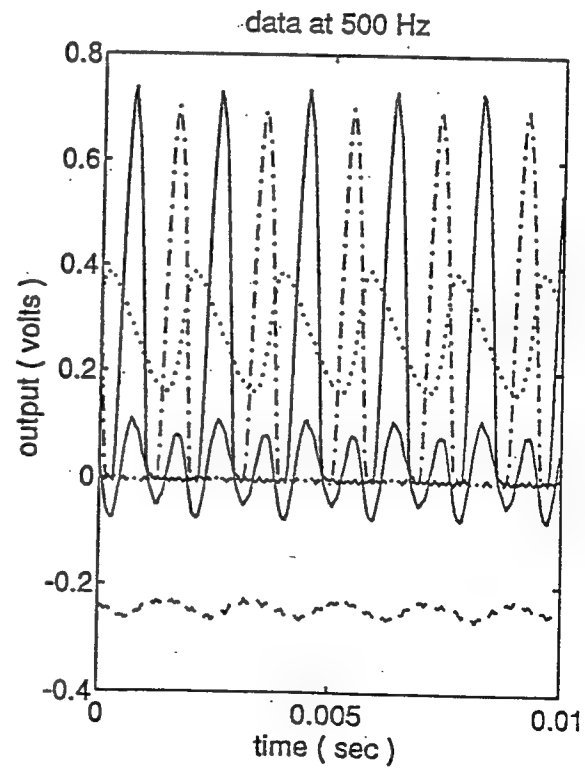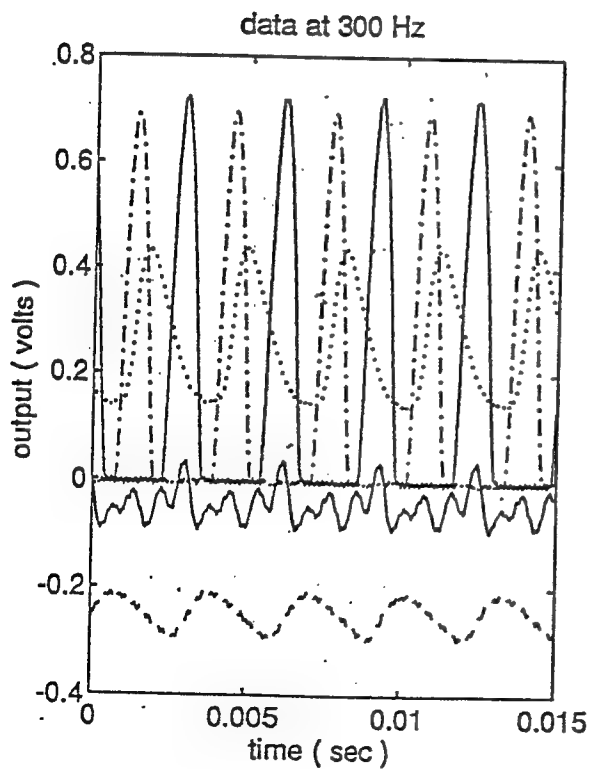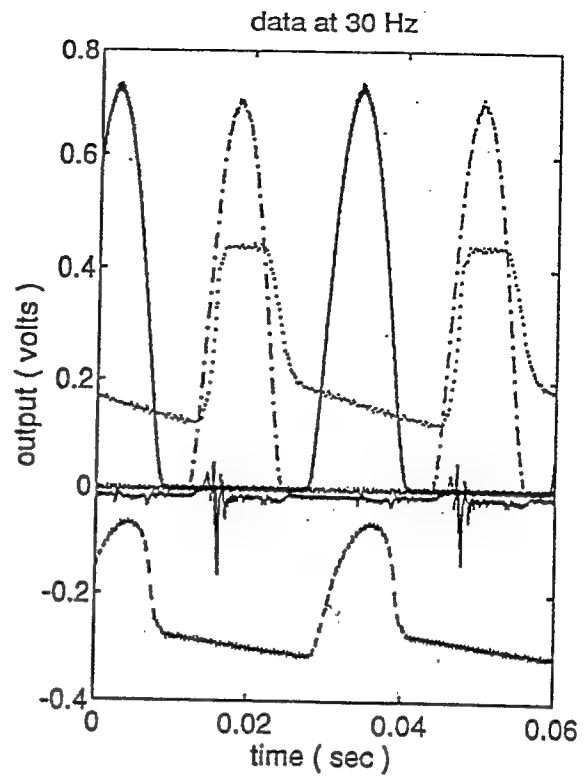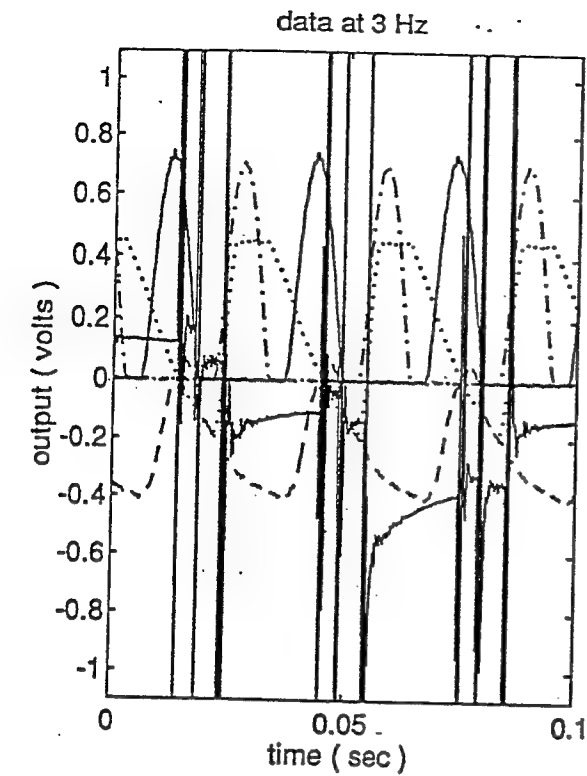
Figure 18: Dynamic test- Experimental results

For all plots: ____: e_1 , -·-·- : e_2 , ----- : i_1 , ... : i_2 . Acceleration data is in solid line.
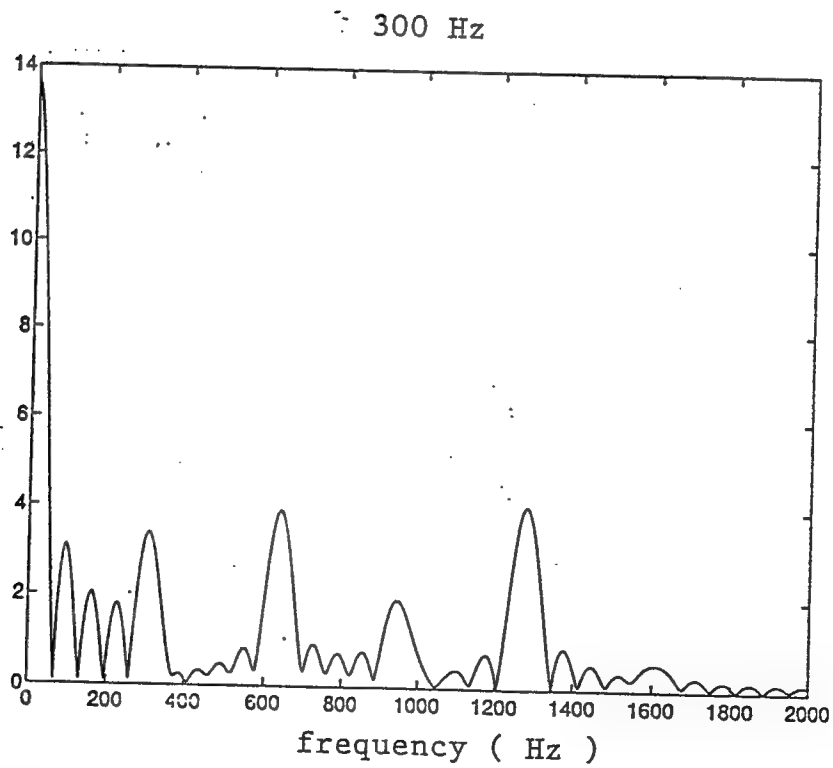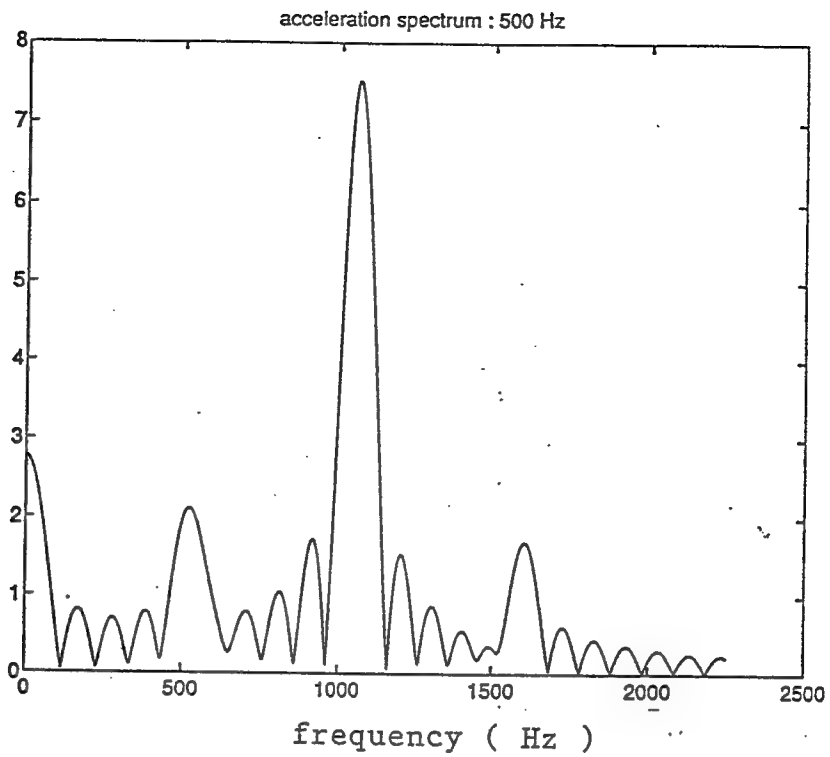
Figure 19: Dynamic test. Acceleration spectrum at 300 Hz and 500 Hz
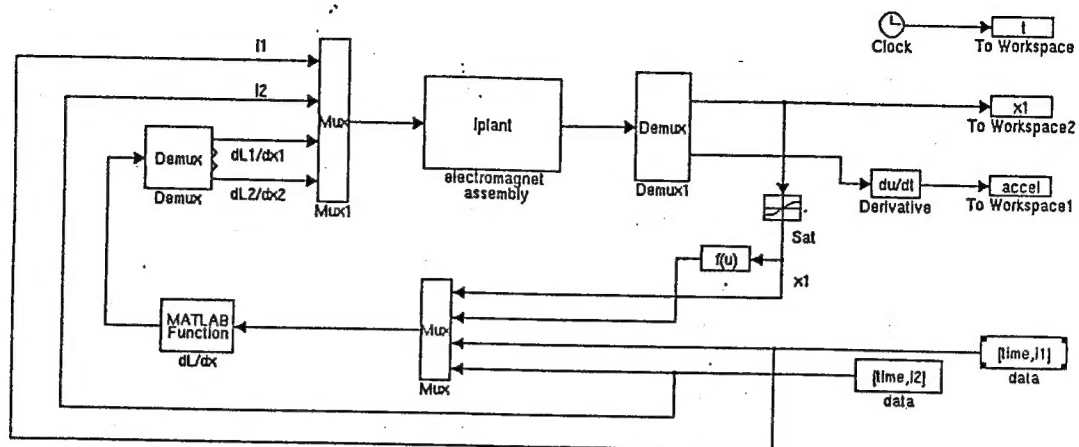
28

Figure 20: Modified simulation network

II.4.2 Simulated acceleration and comparison with actual results

Simulated accelerations corresponding to 300 and 500 Hz data are shown on figure 21. It is remarkable that while the low frequency components seem to match properly, the simulation is unable to track frequencies above 500 Hz.

The poor performance of the simulation network can be attributed primarily to an error on the estimation of circuit parameters (inductances): the approximated calculation can be off by as much as 80% from values predicted using finite-element methods, and even more than that when compared to actual values. The routine implemented for this purpose can be helpful to predict qualitative behavior of the system, but is not dependable when used to estimate actual parameter values. Another parameter uncertainty that need to be considered is the variation on coil resistance with temperature; during the dynamic test described on section 3 considerable heating on the magnet assembly was detected. Finally, heating has a complex effect on the relationship between current and force that has been detected but is not well understood yet.
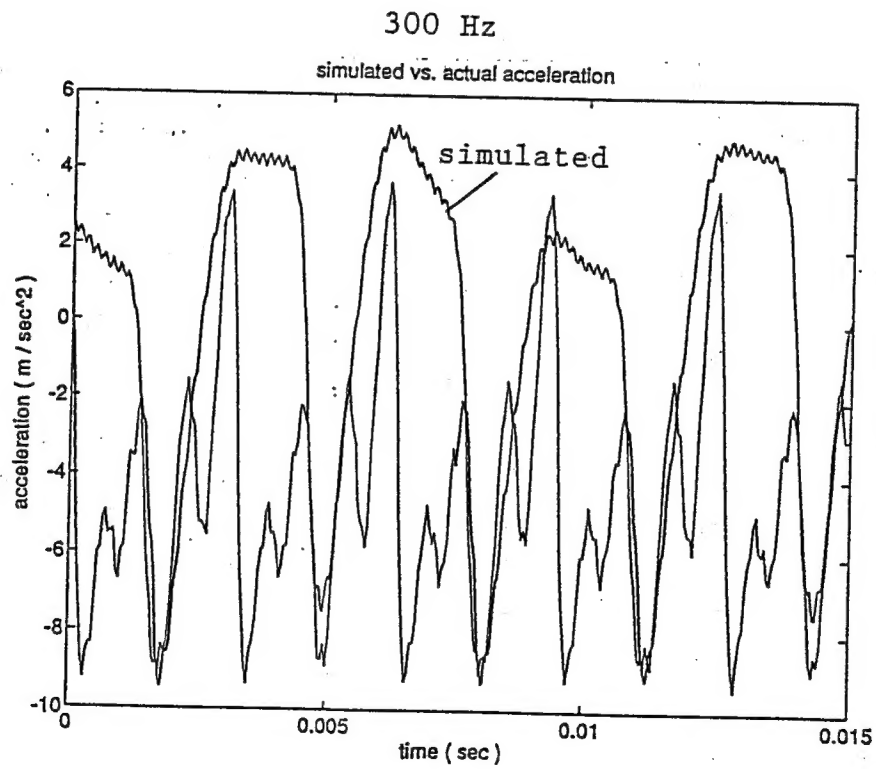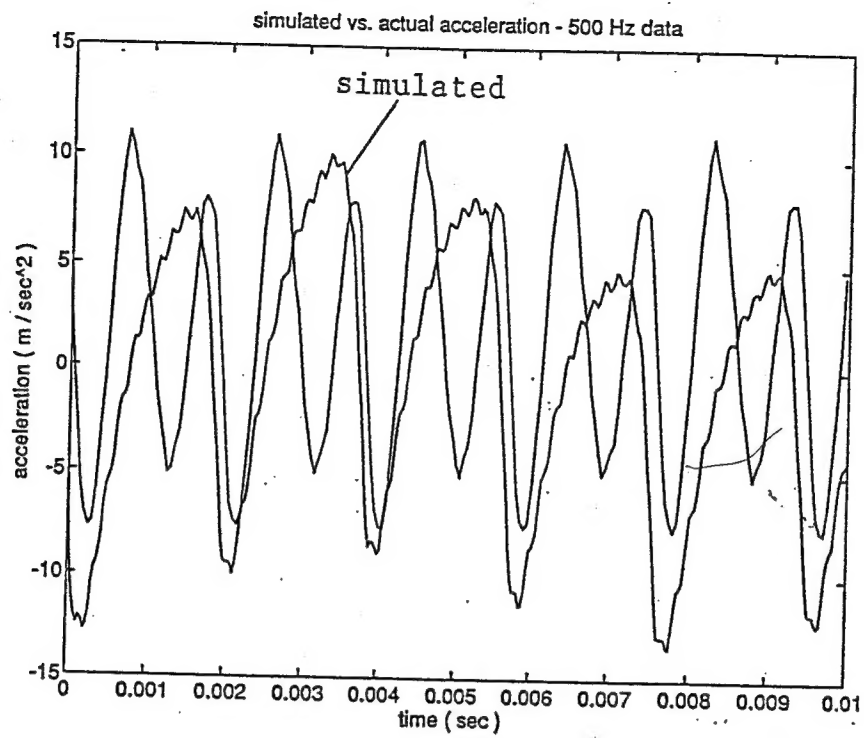
simulated vs. actual acceleration - 500 Hz data

300 Hz

simulated vs. actual acceleration

Figure 21: Comparison between actual and model-generated acceleration

X.8   FUTURE WORK

The most immediate work will revolve around finalizing the static force curves and collecting and analyzing data from the dynamic test fixture. These two areas will be the foundation of further steps to be taken. Final design of the flexures will be the next most important area of research. System modeling using MATLAB and structural analysis using ANSYS will be essential for this process. Flexure design is critical since the range and bandwidth will rely predominantly on them. Finally, heating and counterbalancing issues need to be addressed. Coolant parameters need to be selected so that the magnets can be operated at the design criteria that have been selected. Counterbalancing will need to be addressed to be sure that the DTM remains stable.

Circuit parameter estimation can be improved by the use of finite-element methods: a number of parameter values can be generated for different combinations of position and currents, and the resulting information can be used by any interpolator (e.g. a neural network) to predict inductance values on real time. This method should considerably improve the accuracy on this estimation, although further testing will be required to verify its validity.

The use of neural networks or other intelligent control scheme seems also to be highly recommendable, since modeling the system dynamics to a degree of accuracy that could yield the required performance may turn out to be unfeasible. Intelligent control schemes may be the only practical alternative to overcome modeling uncertainties and highly non-linear behavior. However, it is important to continue working on system modeling, since this is an essential design tool, even to evaluate the feasibility of the proposed performance.

This project is yet at an early stage and several alternatives to carry out system identification, instrumentation, modeling and control will need to be further investigated.

REFERENCES

[1]   Tsuda, M. and T. Higuchi, "Design and Control of Magnetic Servo Levitation", Report of the Institute of Industrial Science, The University of Tokyo, March 1992, Vol.37, No. 2, pp. 137-205.

[2]   Poovey, Tony, Mike Holmes, and David Trumper, "A Kinematically-Coupled Magnetic Bearing Calibration Fixture", *Precision Engineering*, pp.99-108 (1994).

[3]   Bagguley, D. M. *Electromagnetism and Linear Circuits*. Van Nostrand-Reinhold, New York, NY 1973

[4]   Balanis, C. A. *Advanced Engineering Electromagnetics.* John Wiley and Sons, New York, NY 1989

[5]   Goetze, A. J. *Introduction to Electric Power Systems.* North Carolina State University, Dept. of Electrical and Computer Engineering, Raleigh, NC 1993

[6]   Jin, Jian-Ming *The finite-element method in electromagnetics.* John Wiley and Sons, New York, NY 1993.

[7]   Kraus, J. D. *Electromagnetics.* McGraw-Hill, New York, NY 1973.

[8]   Maloney, T. J. *Industrial solid-state electronics: devices and systems.* Prentice Hall, Englewood Cliffs, NJ, 1979

[9]   Phillips, C. L. and Nagle, H.T. *Digital Control System Analysis and Design.* Prentice Hall, Englewood Cliffs, NJ, 1992.

[10]   Ro, P. I. "A mechatronics framework for high precision machining" Proposal approved by the Office of Naval Research Young Investigator Program. North Carolina State University, Raleigh, NC, 1993

[11]   Schwarzenbach, J. and Gill, K. F. *System Modelling and Control.* Edward Arnold, London, 1984

[12]   Wiberg, D. M. *State-space and Linear Systems.* Mc Graw-Hill, New York, NY 1971